Applied Physics Letters

Simultaneous observation of up/down conversion photoluminescence and colossal permittivity properties in (Er+Nb) co-doped TiO_2 materials

Cite as: Appl. Phys. Lett. **109**, 042903 (2016); https://doi.org/10.1063/1.4959829
Submitted: 20 May 2016 . Accepted: 13 July 2016 . Published Online: 27 July 2016

Mei-Yan Tse, Ming-Kiu Tsang, Yuen-Ting Wong, Yi-Lok Chan, and Jianhua Hao

Simultaneous observation of up/down conversion photoluminescence and colossal permittivity properties in (Er+Nb) co-doped TiO_2 materials

Mei-Yan Tse,[1] Ming-Kiu Tsang,[1,2] Yuen-Ting Wong,[1] Yi-Lok Chan,[1] and Jianhua Hao[1,2,a)]
[1]*Department of Applied Physics, The Hong Kong Polytechnic University, Hong Kong, People's Republic of China*
[2]*Shenzhen Research Institute, The Hong Kong Polytechnic University, Shenzhen 518057, People's Republic of China*

(Received 20 May 2016; accepted 13 July 2016; published online 27 July 2016)

We have investigated the optical and dielectric properties of rutile TiO_2 doped with Nb and Er, i.e., $(Er_{0.5}Nb_{0.5})_xTi_{1-x}O_2$. The up/downconversion photoluminescence was observed in the visible and near-infrared region from the materials under 980 nm laser diode excitation. The upconversion emissions are attributed to the energy transfer between Er ions in the excited states. Moreover, the dielectric measurements indicate that the fabricated materials simultaneously present colossal permittivity properties with relatively low dielectric loss. Our work demonstrates the coexistence of both interesting luminescence and attractive dielectric characteristics in (Er+Nb) co-doped TiO_2, showing the potential for multifunctional applications. *Published by AIP Publishing.*
[http://dx.doi.org/10.1063/1.4959829]

Rare-earth (RE) doped materials have attracted considerable interest as they show luminescence not only of Stokes type (downshifting, DS) but also of anti-Stokes type (upconversion, UC) emissions.[1] UC photoluminescence (PL) is a unique physical mechanism, involving sequential absorption of two or more lower excitation photons and resulting in the emission of higher energy photons. The inherent intra-configurational transitions of the RE doped UC materials display superior features, including narrow and sharp 4*f*–4*f* transitions and long-lived luminescence.[2] As a result, these materials have diverse applications in solid state lasers, color displays, optical communications, biosensors,[3] and other photonic devices. Apart from the optical properties, introducing RE ions may improve the dielectric properties of ferroelectric materials. For example, $BaTiO_3$-based perovskites exhibit excellent dielectric properties ($\varepsilon_r \sim 5000$).[4] However, such a high dielectric constant could be attained only at the tetragonal-cubic phase transition temperature ($T_c \sim 120\,^{\circ}C$). The strong temperature dependence of this material limits its applications in electronic devices. Certain RE ions, such as Er^{3+}, Yb^{3+}, Dy^{3+}, and Ho^{3+} have proved to be effective for tuning dielectric and optical properties of barium titanate.[5,6] In addition, the incorporation of Zn^{2+} with Er^{3+}/Yb^{3+} ions was proposed as a promising route to enhance dielectric properties, defect luminescence, and temperature sensing of $BaTiO_3$.[7] Owing to the increasing demand for reliable multifunctional materials, it is essential to conduct further studies on designing hybrid materials using appropriate dopants in various host systems.

Recently, remarkable dielectric behavior was found in (In+Nb) co-doped rutile TiO_2, exhibiting large temperature and frequency independence CP ($\varepsilon_r > 10^4$) as well as a low dielectric loss (<0.05).[8] It is noticeable that the rutile titanium oxide (TiO_2) combines a satisfactory dielectric constant (>100) and an acceptable phonon energy of 612 cm^{-1} to minimize multi-phonon relaxation rates.[9–11] In this regard, the doping of RE ions can improve dielectric properties and meanwhile endow UC and DS properties to the rutile TiO_2. Moreover, those emission wavelengths are useful for lighting and communication applications. However, there has been no exploration of the multifunctional properties in this group of material, including optical and dielectric properties. In this work, $(Er_{0.5}Nb_{0.5})_xTi_{1-x}O_2$ materials were fabricated by solid state sintering method. Structural, optical, and electrical properties are systematically investigated in the $(Er_{0.5}Nb_{0.5})_{0.1}Ti_{0.9}O_2$ ceramics. Importantly, the Er^{3+} dopant employed here acts as not only activator for up/downconversion PL, but also electron acceptor leading to an effective decrease in the loss tangent of dielectrics based on an electron-pinned defect-dipole mechanism.[8] As a result, we have observed simultaneous luminescence and CP properties, which is promising for potential multifunctional applications.

Samples of $(Er_{0.5}Nb_{0.5})_xTi_{1-x}O_2$ at $x = 0\%$ and 10% were prepared by a solid state sintering method. Raw materials, including rutile TiO_2 (99.90%, Sigma-Aldrich), Nb_2O_5 (99.99%, Sigma-Aldrich), and Er_2O_3 (99.5%), were used as received. All of the mixed powders were calcined at 970 °C for 4 h in air. The calcined powders incorporating polyvinyl alcohol (PVA) binder solution were pressed into disks with a diameter of around 12 mm and a thickness of 1.0 mm. Disk samples were then sintered at 800 °C for 2 h in air for removing the PVA binder. The samples were sintered at the temperatures of 1200–1500 °C for 10 h to obtain dense microstructures. The phase structures were confirmed by X-ray diffraction (XRD) and Raman spectroscopy. The optical absorption or reflectance spectroscopy was measured in the spectral range of 200–900 nm using an ultraviolet-visible spectrometer. The PL spectra and lifetime of the samples were recorded by using a FLSP920 spectrometer. An Agilent 4294 A impedance analyzer was used to measure the frequency dependence of dielectric properties over the frequency

a)Author to whom correspondence should be addressed. Electronic mail: jh.hao@polyu.edu.hk

range of 10^2 to 10^5 Hz. All measurements were conducted at room temperature.

Fig. 1(a) shows the XRD patterns of the rutile TiO_2 standard card (JCPDS 65-0191) and $(Er_{0.5}Nb_{0.5})_xTi_{1-x}O_2$ ($x = 10\%$) samples. The results suggest that the samples are of rutile phase, where the small shifting towards low diffraction angle was ascribed to the doping of Er^{3+} and Nb^{5+} ions into the TiO_2 host lattice, resulting in an increased lattice strain. Two secondary phases, Er_2O_3 (JCPDS 26-0604) and $Er_2Ti_2O_7$ (JCPDS 18-0499), were observed in the ceramics. In tetragonal rutile crystals, a Ti^{4+} (radius 0.605 Å) ion associated with six O^{2-} (radius 1.4 Å) ions forms a $[TiO_6]$ octahedron,[12] while Er^{3+} (radius 0.89 Å) and Nb^{5+}(radius 0.64 Å) ions replace Ti^{4+} in lattice to form $[ErO_6]$ and $[NbO_6]$ octahedrons, respectively.[12] As Nb^{5+} ions have similar ionic size with that of Ti^{4+}, it is reasonable that Nb^{5+} ions would preferentially substitute at the Ti^{4+} sites; while the large Er^{3+} ions might thus become "excessive" and result in the secondary phase formation.

Fig. 1(b) presents Raman spectra of $(Er_{0.5}Nb_{0.5})_xTi_{1-x}O_2$ ($x = 0\%$ and 10%) ceramics under 633 nm laser excitation. There are four Raman active fundamental modes in pure rutile TiO_2: B_{1g} (143 cm^{-1}), E_g (447 cm^{-1}), A_{1g} (612 cm^{-1}), and B_{2g} (826 cm^{-1}).[13] B_{1g} corresponds to O–Ti–O bond bending mode, A_{1g} corresponds to Ti–O stretch mode, while E_g mode is due to oxygen atom liberation along the c-axis out of phase.[13] It should be noted that the peak around 240 cm^{-1} was a multi-phonon peak for second-order effect (SOE).[14] Raman spectra of the doped sample show several peaks ranging from 400 to 700 cm^{-1}, similar to the previous studies.[15–17] The result might imply the presence of doped Er^{3+}, Nb^{5+} ions, and Er_2O_3, which is consistent with the XRD patterns.

In order to investigate the optical properties of the fabricated samples, the optical absorption spectrum of the ceramics was initially measured in the Ultraviolet (UV)-to-Near-infrared (NIR) region ranging from 200 to 900 nm as shown in Fig. 2(a). The absorption bands corresponding to the electronic transitions from the $^4I_{15/2}$ ground state to the higher levels $^4I_{9/2}$, $^4F_{9/2}$, $^4S_{3/2}$, $^2H_{11/2}$, and $^4F_{7/2}$ were labeled, respectively.[18] Apparently, the absorption band edge of pure TiO_2 ceramic was present at around 380 nm. Incorporation of Er^{3+} ions into the TiO_2 lattice showed an extended absorption characteristic into the visible region. This may originate from the defects via Er-doping associated with oxygen vacancies

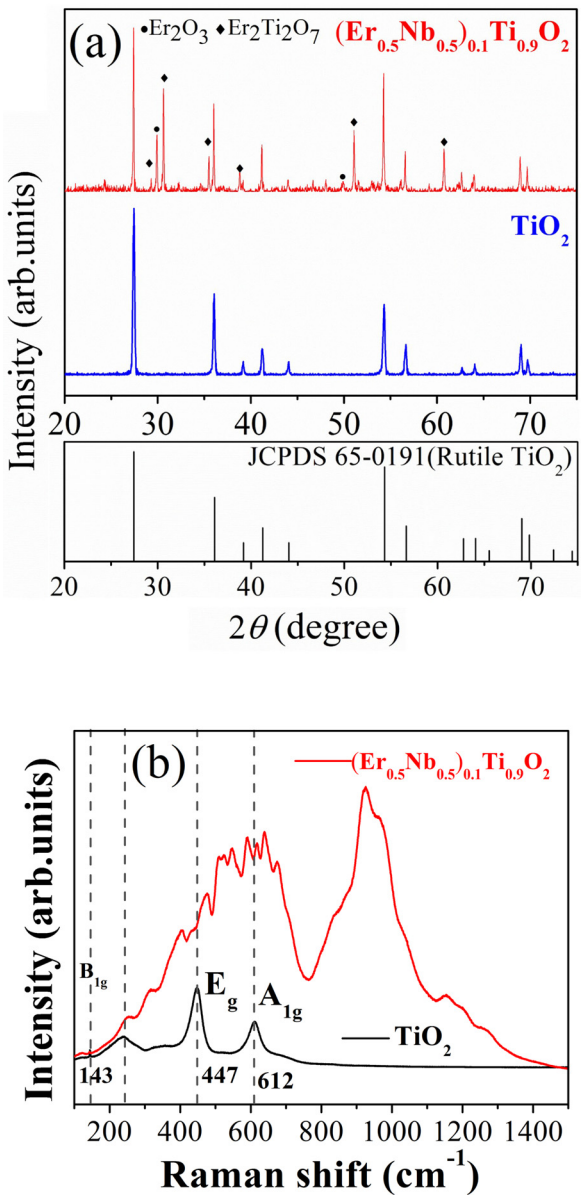

FIG. 1. (a) XRD patterns of the sample $(Er_{0.5}Nb_{0.5})_{0.1}Ti_{0.9}O_2$, pure TiO_2 sintered ceramics, and standard pattern of rutile TiO_2 (JCPDS card 65-0191). (b) Raman spectra of $(Er_{0.5}Nb_{0.5})_xTi_{1-x}O_2$ ($x = 0\%$ and 10%) ceramics.

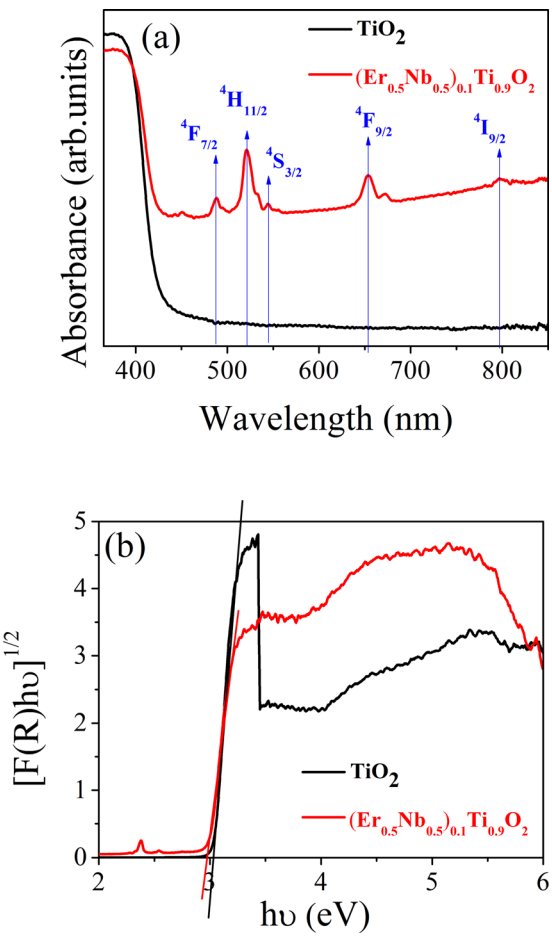

FIG. 2. (a) Optical absorption spectrum and (b) band gap estimation of $(Er_{0.5}Nb_{0.5})_xTi_{1-x}O_2$ ($x = 0\%$ and 10%) ceramics.

that give rise to an F-type color center.[19] The absorbance band edge of the sample $(Er_{0.5}Nb_{0.5})_{0.1}Ti_{0.9}O_2$ ceramics was increased to 392 nm compared with pure TiO_2. It was due to the generation of additional energy levels by the inclusion of impurities within the band gap coupled with oxygen vacancies by metal ion doping. This may contribute to the observed visible light absorption of the co-doped TiO_2 samples.[20]

Fig. 2(b) shows the band gap of pure TiO_2 and $(Er_{0.5}Nb_{0.5})_{0.1}Ti_{0.9}O_2$ ceramics derived from the absorption spectrum. The values were estimated by assuming that the optical absorption of the direct bandgap materials can obey Kubelka–Munk function and Tauc relationship.[21] By extrapolating the linear part of the curve $[F(R)h\nu]^{1/2}$ vs $h\nu$ at $[F(R)h\nu]^{1/2} = 0$, pure TiO_2 ceramic shows the band gap of 3.04 eV, whereas the bandgap of the ceramic at $x = 10\%$ is decreased to 2.97 eV. The narrowing in band gap after Er doping is strongly related to the absorption band of Er^{3+} due to the energy transition of $^4I_{15/2}$ to $^4G_{11/2}$.

Luminescent properties of the materials have played important roles in photonic and biomedicine fields. Therefore, it is interesting to study the luminescence properties of the fabricated materials. Visible UC and NIR DS emissions of the $(Er_{0.5}Nb_{0.5})_{0.1}Ti_{0.9}O_2$ samples are shown in Figs. 3(a) and 3(b), respectively. It is observed that there were two strong green bands in 510–541 nm and 541–580 nm while a weak red band in 640–690 nm under 980 nm diode laser excitation. The green bands correspond to the transitions of $^2H_{11/2} \rightarrow {}^4I_{15/2}$ and $^4S_{3/2} \rightarrow {}^4I_{15/2}$, respectively. The red emission is attributed to the $^4F_{9/2} \rightarrow {}^4I_{15/2}$ transition while the NIR emission band in 1450–1630 nm is assigned to the $^4I_{13/2} \rightarrow {}^4I_{15/2}$ transition of Er^{3+}. These emission wavelengths are well-known for modern optical communication and optoelectronic devices. All the emission bands are split into two obvious peaks, which are ascribed to the Stark splitting of the degenerate 4*f* levels under the crystal field. Moreover, the pumping power dependence of visible UC and NIR DS intensity was investigated to understand the PL nature. For an unsaturated UC process, the number of photons that is necessary to populate the upper emitting state can be obtained by $I_{UC} \propto (P_{pump})^n$,[22] where I_{UC} is the integrated fluorescence intensity, P_{pump} is the pumping power, and n is the number of laser photons required to produce one UC photon. The insets of Figs. 3(a) and 3(b) show the double logarithmic plots of the overall emissions at 522, 557, 656, and 1492 nm as a function of pumping power. The n value can be calculated from the slope of the linear fit (inset of Fig. 3(a)). The obtained n of the samples for the green transitions of $^2H_{11/2} \rightarrow {}^4I_{15/2}$ and $^4S_{3/2} \rightarrow {}^4I_{15/2}$ was 1.48 and 1.27, respectively, implying the two photon processes of the green UC PL.[7] The slope value of $^4F_{9/2} \rightarrow {}^4I_{15/2}$ transition was 1.13. This decreased n value could be explained by the cross relaxation of the $^4F_{9/2}$ level.[7] For the $^4I_{13/2} \rightarrow {}^4I_{15/2}$ transition, the slope value with $n = 1$ shows that this state was populated via single photon absorption from the ground state for NIR DS emission.

Apart from the pump power dependence analysis, another useful tool to investigate the PL mechanism is to study the temporal behavior of UC PL under a pulse excitation. This technique allows one to distinguish between

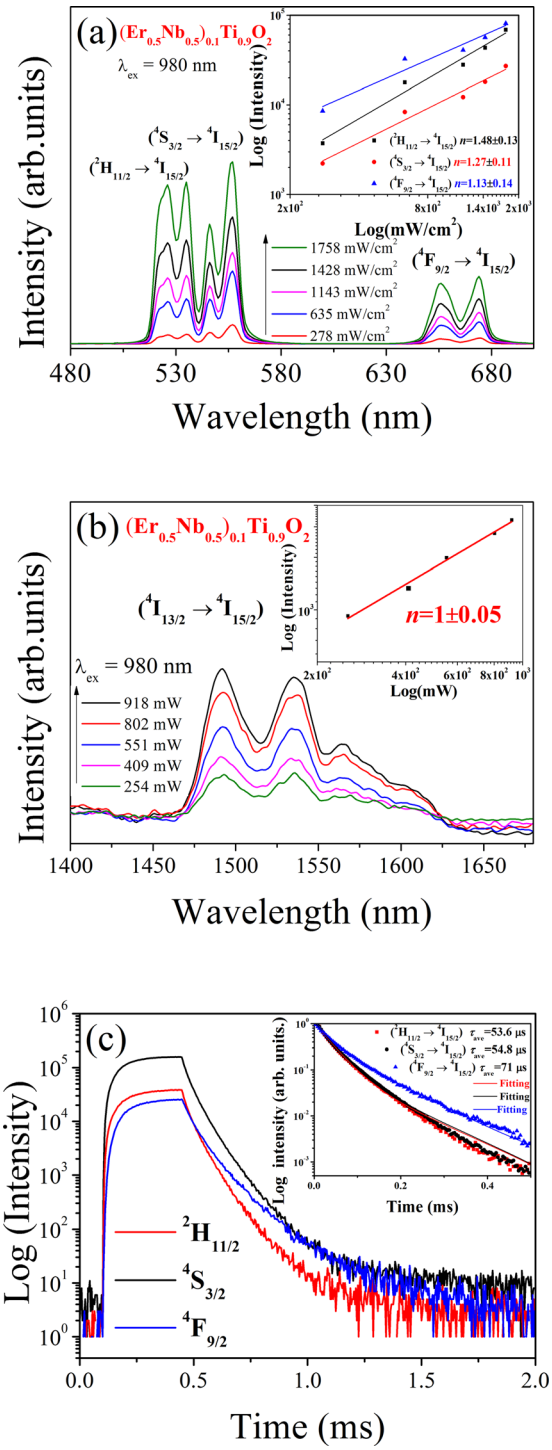

FIG. 3. (a) Visible UC and (b) NIR DS emission spectra of the $(Er_{0.5}Nb_{0.5})_{0.1}Ti_{0.9}O_2$ ceramic under 980 nm laser excitation with various pumping power; the inset shows the respective log–log plots in visible UC and NIR DS emission intensity versus excitation power density in the ceramics. (c) Temporal behavior of UC PL from the $^2H_{11/2}$, $^4S_{3/2}$, and $^4F_{9/2}$ levels under the 980 nm laser excitation in a semi-logarithmic representation; the inset shows various UC PL decay curves of Er^{3+} ions with the fitting (solid lines).

excited state absorption (ESA) and energy transfer upconversion (ETU) processes.[23–25] The typical signature of an ESA process is an exponential decay, whereas the signature of an ETU process is a rise followed by an exponential decay. Fig. 3(c) shows the temporal behavior of UC PL from the $^2H_{11/2}$, $^4S_{3/2}$, and $^4F_{9/2}$ levels under the laser excitation at 980 nm;

the inset shows the decay curves of the sample at 522, 557, and 656 nm. The decay time was found from the slope of a plot of log I (t) versus t. The curve was well fitted by the double exponential equation[26,27]

$$I(\mathrm{t}) = I_0 + A_f e^{\left(-\frac{t-t_0}{\tau_f}\right)} + A_s e^{\left(-\frac{t-t_0}{\tau_s}\right)}, \quad (1)$$

where I is the luminescence intensity, τ_f and τ_s are the fast and slow components of the luminescent lifetimes, A_f and A_s are the weight factors of the two components, respectively, and t_0 is the initial delay of the measurement. The average lifetime of the non-exponential decay curve is determined by the expression[27]

$$\tau_{ave} = \frac{A_f\tau_f^2 + A_s\tau_s^2}{A_f\tau_f + A_s\tau_s}. \quad (2)$$

Typical ETU behaviors for both green and red UC emissions were observed (Fig. 3(c)). The temporal behavior of UC PL from the $^2H_{11/2}$, $^4S_{3/2}$, and $^4F_{9/2}$ levels shows a rise profile at initial stage followed by a double exponential decay behavior. Two time components of the decay are noticeable in the semi-logarithmic plot (inset of Fig. 3(c)). The fast component derives a lifetime of 35 μs, while the lifetime of the slow component is found to be 107 μs for $^2H_{11/2}\rightarrow{}^4I_{15/2}$ transition. The fitting results associated with $^4S_{3/2}\rightarrow{}^4I_{15/2}$ show $\tau_f = 36\,\mu$s and $\tau_s = 105\,\mu$s, whereas $\tau_f = 33\,\mu$s and $\tau_s = 94\,\mu$s correspond to $^4F_{9/2}\rightarrow{}^4I_{15/2}$. The above analysis shows the presence of two emitting species. It can be implied that ETU is a dominant mechanism for the UC emissions in the material system yet an ESA process could not be ruled out.

The spectroscopic properties and mechanisms of UC PL of Er^{3+} ions vary with the material's preparation and excitation conditions.[28,29] Based on the results of pump power dependence and decay curves, a simplified energy level diagram is proposed to illustrate the mechanisms (Fig. 4). The mechanism of UC under the excitation at 980 nm is explained by a previous study.[1] The observed luminescent properties of the (Er+Nb) co-doped TiO_2 are similar to other reports, such as Er^{3+}-doped $BaTiO_3$ and Er^{3+}/Yb^{3+} co-doped $PbTiO_3$.[30,31]

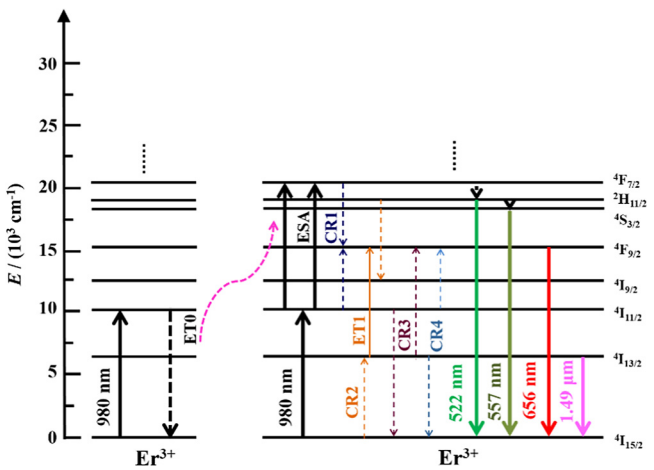

FIG. 4. Simplified energy level diagram of Er^{3+} ion depicting the proposed mechanisms for the various UC and NIR DS emissions under 980 nm excitation.

In this work, red UC emissions related to the $^4F_{9/2}$ excited state are relatively weak. It may be due to a relatively large energy separation between the $^4F_{9/2}$ and $^4S_{3/2}$ state, which is about five times the phonon energy of the TiO_2 lattice (612 cm^{-1}). Therefore, the red emission state of $^4F_{9/2}$ might be populated via another route. Fig. 4 shows several representative processes of the cross relaxation (CR) processes. First, CR1, i.e., $^4F_{7/2} + {}^4I_{11/2}\rightarrow{}^4F_{9/2} + {}^4F_{9/2}$. As Er^{3+} ion populated to the $^4F_{7/2}$ level would relax to the $^2H_{11/2}$, $^4S_{3/2}$ state by multi-phonon relaxation, the state density of $^4F_{7/2}$ state for CR1 is low; this process might not be the foremost one for the red emission. Second, $^2H_{11/2}/{}^4S_{3/2} + {}^4I_{15/2}\rightarrow{}^4I_{9/2} + {}^4I_{13/2}$ for CR2. The Er^{3+} ions at $^4I_{13/2}$ state through ET populate the $^4F_{9/2}$ state. As the green emissions for Er^{3+} are relatively high, it implies that the state density of the $^2H_{11/2}/{}^4S_{3/2}$ states is high. CR2 may lead to the red emission efficiently. Lastly, CR between lower states, CR3: $^4I_{11/2} + {}^4I_{13/2}\rightarrow{}^4F_{9/2} + {}^4I_{15/2}$ or CR4: $^4I_{13/2} + {}^4I_{11/2}\rightarrow{}^4F_{9/2} + {}^4I_{15/2}$. If they are amenable, the intensity of red emission should be higher than that of green one. In other words, CR from lower states forms a minor process for the red emission. It can be concluded that the red UC emission is attributed to the CR2 ($^2H_{11/2}/{}^4S_{3/2} + {}^4I_{15/2}\rightarrow{}^4I_{9/2} + {}^4I_{13/2}$). Most of the Er^{3+} ions in the $^4I_{13/2}$ level will eventually relax radiatively to the $^4I_{15/2}$ level, generating the 1.55 μm NIR emission. As most of the Er^{3+} ions are expected to excite to the higher energy levels, the low photon transition probability of $^4I_{13/2}$ levels is small. Eventually, the NIR emissions become very weak.

As aforementioned, co-doping Nb^{5+} and Er^{3+} ions may result in remarkable dielectric properties in addition to the above interesting optical properties. Fig. 5 shows the frequency-dependent dielectric properties of pure TiO_2 and $(Er_{0.5}Nb_{0.5})_{0.1}Ti_{0.9}O_2$ ceramics at room temperature. A relatively low ε_r (~800) was observed in pure TiO_2. In contrast, the magnitude of ε_r was significantly enhanced up to ~6 × 10^4 while low dielectric loss was evident when co-doping Nb^{5+} and Er^{3+} ions into the TiO_2 host. The permittivity of the doped sample was almost steady and its dielectric loss can meet the requirement ($<10^{-1}$) with varied frequencies.[32–34] The results indicate weak frequency dependence of the doped sample. In this study, Er^{3+} ions act as the electron acceptor for holding back the delocalized electrons while

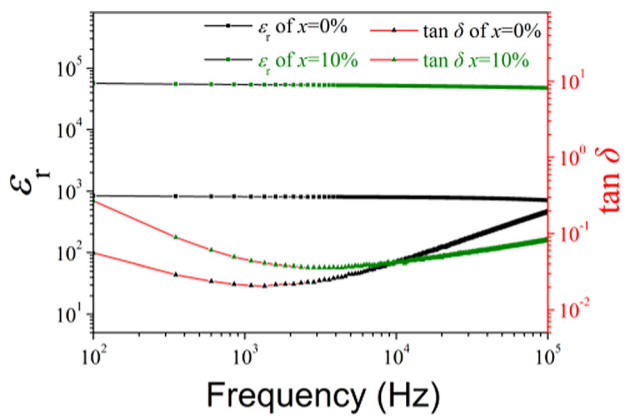

FIG. 5. Dielectric properties of $(Er_{0.5}Nb_{0.5})_xTi_{1-x}O_2$ ($x = 0\%$ and 10%) ceramics in the frequency range of 10^2 to 10^5 Hz, measured at room temperature.

Nb^{5+} substitution creates delocalized electrons from the reduction of Ti^{4+}. This physical mechanism responsible for such high-performance dielectric properties is similar to our previously reported system of (Zn, Nb) co-doped TiO_2.[35]

In conclusion, $(Er_{0.5}Nb_{0.5})_{0.1}Ti_{0.9}O_2$ material was fabricated by a solid state sintering method. Green, red, and NIR emission were obtained from the material under 980 nm laser excitation based on an up/downconversion photon process. Furthermore, co-doping Er^{3+} and Nb^{5+} ions in TiO_2 is found to greatly enhance the CP performance with low dielectric loss. The results suggested that co-doping Er^{3+} and Nb^{5+} ions is a promising route to generate the multi-functionality of TiO_2 host material composed of remarkable luminescence and dielectric properties.

This work was supported by grants from the Research Grants Council of Hong Kong (GRF No. PolyU 153004/14 P) and National Natural Science Foundation of China (Grant No. 11474241).

[1]F. Auzel, Chem. Rev. **104**, 139 (2004).
[2]M.-K. Tsang, G. Bai, and J. Hao, Chem. Soc. Rev. **44**, 1585 (2015).
[3]M.-K. Tsang, W. Ye, G. Wang, J. Li, M. Yang, and J. Hao, ACS Nano **10**, 598 (2016).
[4]M. T. Buscaglia, M. Viviani, V. Buscaglia, L. Mitoseriu, A. Testino, P. Nanni, Z. Zhao, M. Nygren, C. Harnagea, D. Piazza, and C. Galassi, Phys. Rev. B **73**, 064114 (2006).
[5]B. Li, S. Zhang, X. Zhou, Z. Chen, and S. Wang, J. Mater. Sci. **42**, 5223 (2007).
[6]A. Y. Fasasi, M. Maaza, E. G. Rohwer, D. Knoessen, Ch. Theron, A. Leitch, and U. Buttner, Thin Solid Films **516**, 6226 (2008).
[7]M. K. Mahata, T. Koppe, T. Mondal, C. Brüsewitz, K. Kumar, V. K. Rai, H. Hofsässa, and U. Vettera, Phys. Chem. Chem. Phys. **17**, 20741 (2015).
[8]W. Hu, Y. Liu, R. L. Withers, T. J. Frankcombe, L. Norén, A. Snashall, M. Kitchin, P. Smith, B. Gong, H. Chen, J. Schiemer, F. Brink, and J. Wong-Leung, Nat. Mater. **12**, 821 (2013).
[9]C. T. Dervos, E. F. Thirios, J. Novacovich, P. Vassiliou, and P. Skafidas, Mater. Lett. **58**, 1502 (2004).
[10]I. P. Suzdalev, V. E. Prusakov, Yu. V. Maksimov, V. K. Imshennik, S. V. Novochikhin, E. A. Gudilin, A. V. Grigor'eva, K. L. Dubova, S. S. Abramchuk, Yu. D. Tret'yakov, I. S. Lyubutin, and K. D. Frolov, Nanotechnologies in Russia **5**, 223 (2010).
[11]R. Balda, A. J. Garcia-Adeva, M. Voda, and J. Fernández, Phys. Rev. B **69**, 205203 (2004).
[12]R. T. Shannon, Acta Crystallogr. A **32**, 751 (1976).
[13]X. Cheng, Z. Li, and J. Wu, J. Mater. Chem. A **3**, 5805 (2015).
[14]Y. Zhang, C. X. Harris, P. Wallenmeyer, J. Murowchick, and X. Chen, J. Phys. Chem. C **117**, 24015 (2013).
[15]J. Cui and G. A. Hope, J. Spectrosc. **2015**, 940172.
[16]A. J. Barbosa, F. A. D. Filho, L. J. Q. Maia, and Y. Messaddeq, J. Phys.: Condens. Matter **20**, 285224 (2008).
[17]A. Ceja-fdez, T. López-luke, J. Vivero-escoto, A. L. Gonzalez-Yebra, R. A. R. Rojas, A. Martínez-pérez, A. Ceja-fdez, T. López-luke, J. Oliva, J. Vivero-escoto, and A. L. Gonzalez-Yebra, J. Biomed. Opt. **20**, 046006 (2015).
[18]V. O. Obadina and B. R. Reddy, Opt. Photon. J. **3**, 45 (2013).
[19]J. Chen, L. B. Lin, and F. Q. Jing, J. Phys. Chem. Solids **62**, 1257 (2001).
[20]J. Choi, H. Park, and M. R. Hoffmann, J. Phys. Chem. C **114**, 783 (2010).
[21]S. Som, M. Chowdhury, and S. K. Sharma, J. Mater. Sci. **49**, 858 (2014).
[22]F. Pandozzi, F. Vetrone, J.-C. Boyer, R. Naccache, J. A. Capobianco, A. Speghini, and M. Bettinelli, J. Phys. Chem. B **109**, 17400 (2005).
[23]M. Pollnau, D. R. Gamelin, S. R. Lüthi, and H. U. Güdel, Phy. Rev. B **61**, 3337 (2000).
[24]M. P. Hehlen, G. Frei, and H. U. Güdel, Phy. Rev. B **50**, 16264 (1994).
[25]T. Riedener and H. U. Güdel, J. Chem. Phys. **107**, 2169 (1997).
[26]H. X. Zhang, C. H. Kam, Y. Zhou, X. Q. Han, S. Buddhudu, Q. Xiang, Y. L. Lam, and Y. C. Chan, Appl. Phys. Lett. **77**, 609 (2000).
[27]S. L. Dong, H. H. Lin, T. Yu, and Q. Y. Zhang, J. Appl. Phys. **116**, 023517 (2014).
[28]F. Wang, Y. Han, C. S. Lim, Y. Lu, J. Wang, J. Xu, H. Chen, C. Zhang, M. Hong, and X. Liu, Nature **463**, 1061 (2010).
[29]Y. Wang, G. Liu, L. Sun, J. Xiao, J. Zhou, and C. Yan, ACS Nano **7**, 7200 (2013).
[30]Y. Zhang, J. Hao, C. L. Mak, and X. Wei, Opt. Express **19**, 1824 (2011).
[31]F. C. D. Lemos, D. M. A. Melo, and J. E. C. da Silva, Mater. Res. Bull. **40**, 187 (2005).
[32]Z. Gai, Z. Cheng, X. Wang, L. Zhao, N. Yin, R. Abah, M. Zhao, F. Hong, Z. Yu, and S. Dou, J. Mater. Chem. C **2**, 6790 (2014).
[33]P. Lunkenheimer, S. Krohns, S. Riegg, S. G. Ebbinghaus, A. Reller, and A. Loidl, Eur. Phys. J. Spec. Top. **180**, 61 (2009).
[34]C. C. Homes and T. Vogt, Nat. Mater. **12**, 782 (2013).
[35]X. Wei, W. Jie, Z. Yang, F. Zheng, H. Zeng, Y. Liu, and J. Hao, J. Mater. Chem. C **3**, 11005 (2015).